IN-SITU INTIMATE CONTACT EVALUATION IN FUSED FILAMENT FABRICATION

Correa, A.[1]*, Lengaigne, J.[1], Smith, A[1]., Tabiai, I[1], Dubé, M.[1]
[1] CREPEC, Department of Mechanical Engineering, École de Technologie Supérieure, Montréal, Canada.
* Corresponding author (andre.rittner-pires-correa.1@ens.etsmtl.ca).

Keywords*: FFF, contact signature, in-situ* and *ex-situ* analysis.

ABSTRACT

Fused filament fabrication (FFF), also known as fused deposition modelling, is one of the most commonly used additive manufacturing techniques for thermoplastic polymers. In this process, filament feedstock is pushed through a heated nozzle, which both melts the polymer and controls the amount of material deposited onto a sometimes-heated substrate. A 3-dimensional component is created by layering rows of material and often consists of an external shell and internal porous infill to limit part density. Initially introduced as a fast prototyping tool, FFF may yet be relevant for load-bearing structural applications if the relationships between processing parameters, mechanical performance and dimensional stability can be better understood. While final part quality depends on a plethora of process and material parameters, the most common source of print failure is a weak bond between the first print layer and the build plate. In this work, a custom *in-situ* optical set-up comprised of a modified commercial FFF printer and a DSRL camera is used to image the interface between a layer of PLA and a transparent build plate. Different lighting conditions are tested to obtain an image with as much detail as possible. *Ex-situ* observations under optical and confocal microscopy are used to correlate the grey-scale signals obtained by *in-situ* observations with the possible contact of the deposited filament.

1 INTRODUCTION

Additive manufacturing (AM) has attracted unprecedented attention in a number of industries due to its potential for use in rapid prototyping of 3D complex parts. As opposed to traditional subtractive machining techniques, AM generally begins with the design of a 3D virtual model that is sliced into several 2D horizontal cross-sections using a slicing software. By successively printing new 2D layers on top of previous layers, a coherent 3D object can be finally fabricated with near-zero material waste [1]. Fused filament fabrication (FFF) is one of the most widespread AM methods thanks to economic accessibility, ease of use and a vast amount of commercially available feedstock [2]. As depicted in Figure 1, this process involves feeding polymer filament into a heated block, where the material is softened or melted. The material is then extruded in a semi-cylindrical form onto a sometimes heated building plate. The extrusion temperature must be sufficiently high to allow material flow, layer wetting and interface healing, but minimally low to avoid structural collapse – due to the lower material viscosity at high temperatures – or material degradation. Upon the deposition, the incoming filament immediately begins to cool down, exchanging heating by convection with the surrounding air and conduction with the substrate or previous layers, and eventually solidifies, preventing material to flow. Once a layer is extruded, the distance between the nozzle and the platform is increased for the next layer of material to be extruded. At every and each new layer deposition, the previous layers are re-heated, creating a complex dynamic thermo-mechanical problem. This layer-by-layer manufacturing process is carried out until the 3D part is completed.

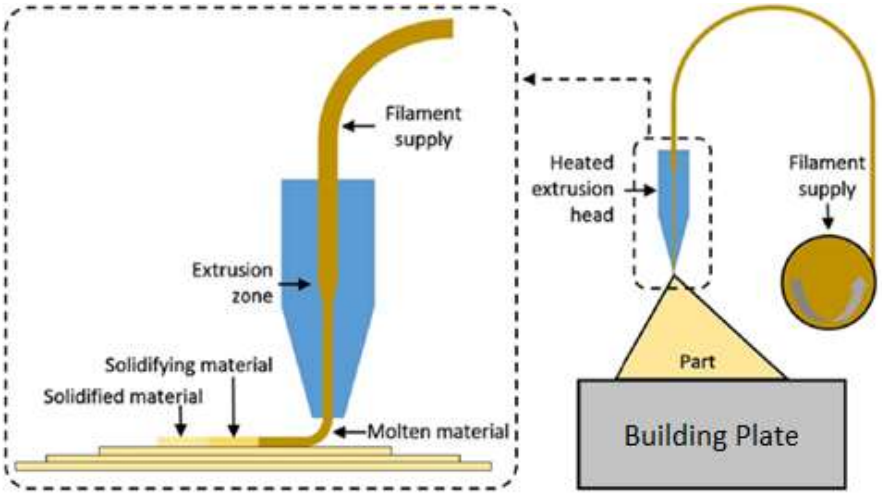

Figure 1: Schematic representation of the FFF process. Adapted from [1].

The quality of the final part depends on a large number of parameters, such as the filament quality, printing temperature, extrusion rate, printing velocity, etc. The most common source of print failures is a weak bond between the first print layer and the build plate [2]. First-layer print failures can occur due to irregular plate levelling, improper distancing between the extrusion nozzle and build plate, excessively high printing speed and inappropriate extrusion and building plate temperature miss-match, creating internal thermal stresses. Different authors have worked on identifying and monitoring FFF failures. Wu *et al.* [3], Li *et al.* [4] and Yang *et al.* [5] proposed the usage of acoustic emissions to identify and monitor printing failures, warpage distortions and filament breakage. Kousiatza and Karalekas [6] used fibre Bragg grating sensors for *in-situ* strain field monitoring and to develop temperature profiles during an FDM print. Li *et al.* [7] used vibration sensors and data-driven methods to recognize and monitor print defects. Finally, Paraskevoudis *et al.* [8] suggested the usage of computer vision and artificial intelligence to detect stringing during FFF print.

Though significant work has been performed for printer monitoring, little has been done to identify first-layer bond failures. The goal of this paper is to present a simple method for *in-situ* characterization of first-layer print failures that can be easily integrated into existing FDM machines. To this end, a preliminary work using an optical setup to identify the contacting signatures between the first-layer and the building plate is presented002E The results shown suggest that this method can be effectively used for *in-situ* first-layer inspection during FFF printing. Moreover, the results provide insights into the deformation, thermal and flow history of the deposited filament.

2 METHODOLOGY

2.1 Sample Preparation

A simple representative sample was used throughout this investigation. This sample was prepared by extruding a single layer of 1.75 mm diameter PLA filament from 3DXtech using an Ender-3 FFF machine from Creality 3D equipped with a 0.4 mm nozzle. The PLA was dried out for 24 h prior to printing. The printing parameters included an extrusion temperature of 210 °C and a print speed of 25 mm-s^{-1}.

2.2 In-situ FFF Observation

Figure 2 presents the setup used for this study. It consists of an optical acquisition system embedded in a modified FFF machine. Several structural modifications were performed: the replacement of the original building plate by a transparent glass, a support for holding a LED strip and an overhang to hold the building plate far from the printer base to allow the installation of the optical components. The optical acquisition system consists of a digital camera facing a 45º mirror under the build plate, with three different light sources: a top LED strip, a bottom LED panel and a side LED illuminator. The mirror was placed between the printer frame and the suspended glass plate, redirecting the light coming from the sample to the camera. For this experiment, a Canon 500D DSLR camera mounted with a Sigma 105mm F2.8 macro lens was positioned at a predefined distance from the mirror. The LED strip was placed on the printed support facing the building plate, in a way that the emitted light is transmitted through the sample that is being printed. The LED panel is positioned facing the bottom face of the glass plate, in a way that the emitted light is reflected by the sample that is being printed. Finally, the LED illuminator emits in-plane light at a 45º of the glass plate.

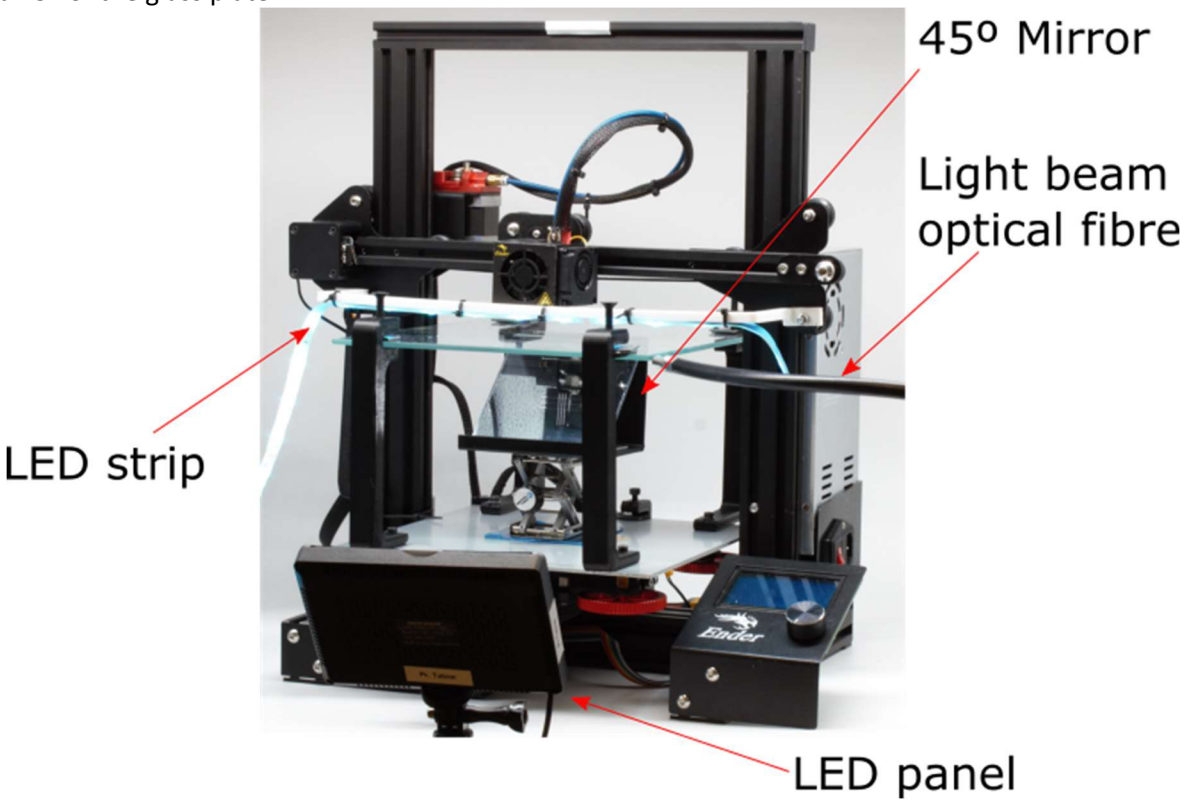

Figure 2. Modified Ender 3 printer, instrumented with an optical acquisition system

Given the apparatus described above, an experimental campaign was carried out to determine what combination of lighting conditions allows for the best observation of first layer contact. Three locations of the deposited filament were used as references for the regions of interest (ROI) and are named as head (region closer to the beginning of the deposition), middle (central region) and trailing (region closer to the end of the deposition). The print was recorded using the DSLR camera after the deposition of the specimen on the glass plate. The LED strip has a maximum power of 18 W, the LED panel 10 W and the illuminator 120W (2000+lumens). A test matrix, varying the power of each of the light sources, was created and shown in Table 1. The 18 different light conditions, obtained from all the permutations of the testing matrix shown in Table 1, were tested and evaluated. Illumination conditions

are named using the percentage of light power for each source in order (transmitted, in-plane, reflected), for example: 50/100/50, indicates 50% of transmitted power, 100 % of in-plane and 50% of reflected.

Table 1. Illumination parameters used for the test matrix

Transmitted (LED strip)	In-plane (beam generator)	Reflected (LED panel)
100 %	100 %	100 %
0 %	50 %	44 %
-	0 %	0 %

2.3 Ex-situ observation

After the *in-situ* campaign, the sample was imaged *ex-situ* to compare and to correlate the observed signatures. The sample was observed under a conventional optical microscope (Nikon eclipse MA100M, LE plan 5x/0.1, TS2-W10x). In addition, the sample was characterized with a confocal laser microscope (Olympus LEXT OLS5500) to obtain a 3D profile of the bed/filament interface.

2.4 Image Processing

The raw images captured either by the *in-situ* acquisition system or by the *ex-situ* optical microscope were analyzed using ImageJ. As described in Figure 3, the images were imported as a stack and converted into 32-bits grey-scale images. An evaluation window, covering the full width of the filament at each ROI, was opened. The grey-scale intensity signal at each ROI was averaged over the width of the ROI to obtain an intensity profile. Finally, the intensity profile through the filament width inside this evaluation window was extracted and used for feature identification and comparison.

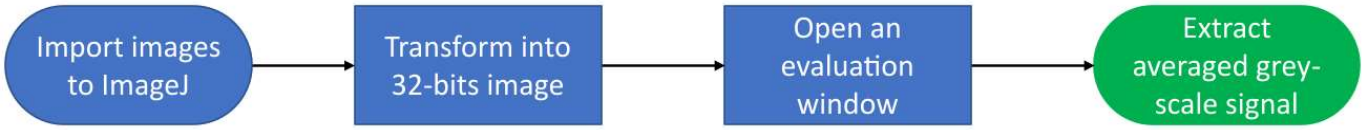

Figure 3: Experimental block diagram.

3 RESULTS

3.1 In-situ FFF Observation

Figure 4 shows the measured grey-scale intensity across the head of the filament width for the different light conditions. One can observe that the signal response is sensitive to the light condition, significantly differing from one to the other. Particularly to this ROI, the conditions in which no reflected light was combined with considerable in-plane light were able to reproduce features that are visibly defined, while the others did not show any significant signal changes. These features correspond to the two troughs at the width extremities, followed by two internal peaks and subsequent troughs.

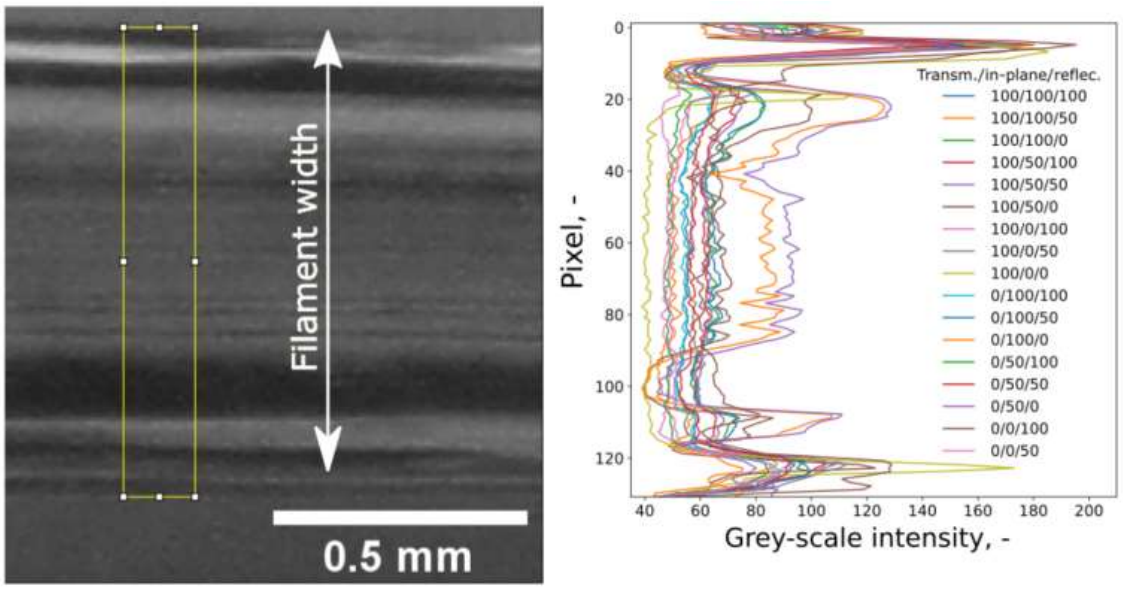

Figure 4: Extracted grey-scale intensity through the width of the filament at the head ROI (right) from the first-layer (left) to substrate contact signature. An evaluation window (in yellow) is opened and values are averaged. Several dark/bright features in the left image are translated in trough/peak grey-scale intensity.

Figure 5 shows the same results but singling out the conditions in which those features are not magnified in the grey-scale intensity. As mentioned, the remaining conditions have a considerable amount of in-plane light and complete absence of reflected light. When comparing the left image to the graph, one can observe that the bright regions are identified by the peaks while the dark regions correspond to the troughs.

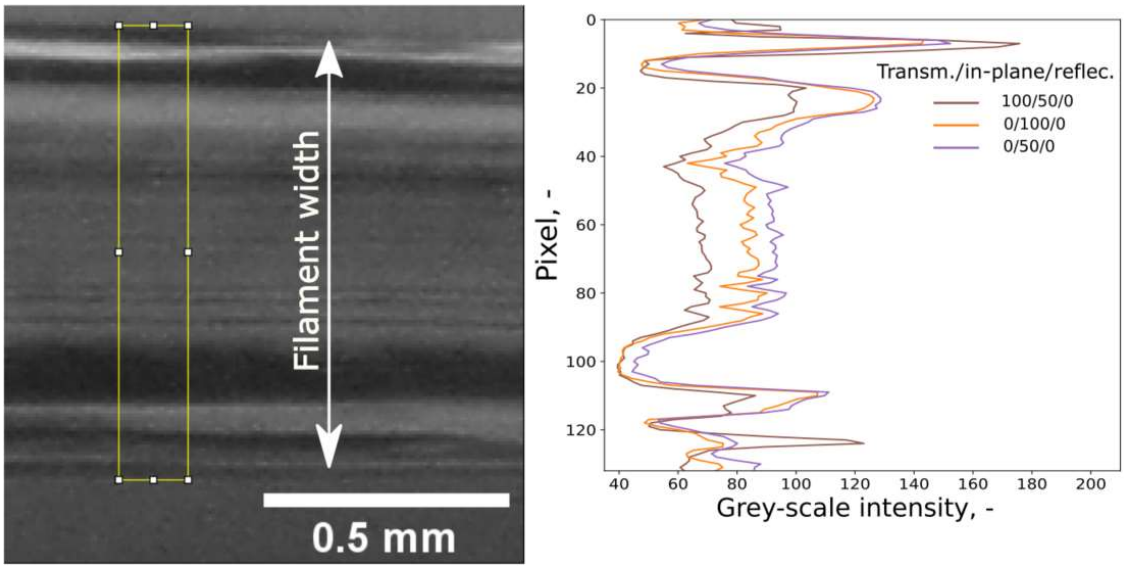

Figure 5: Most reactive grey-scale curves at the head ROI (right) from the first-layer (left) to substrate contact signature. A clear correlation of dark/bright zones to trough/peaks inside the evaluation window are observed.

Like for the head, the centred part of the filament was evaluated. At this ROI, the effect of the nozzle being captured in the image was studied. It is believed that the nozzle may reflect part of the surrounding stray light,

significantly disturbing the measurements. It is important to consider this effect, since in a dynamic scenario, the nozzle would constantly pass on top of the filament. The grey scale intensity was extracted from an evaluation window that was opened immediately before the nozzle as shown in Figure 6.

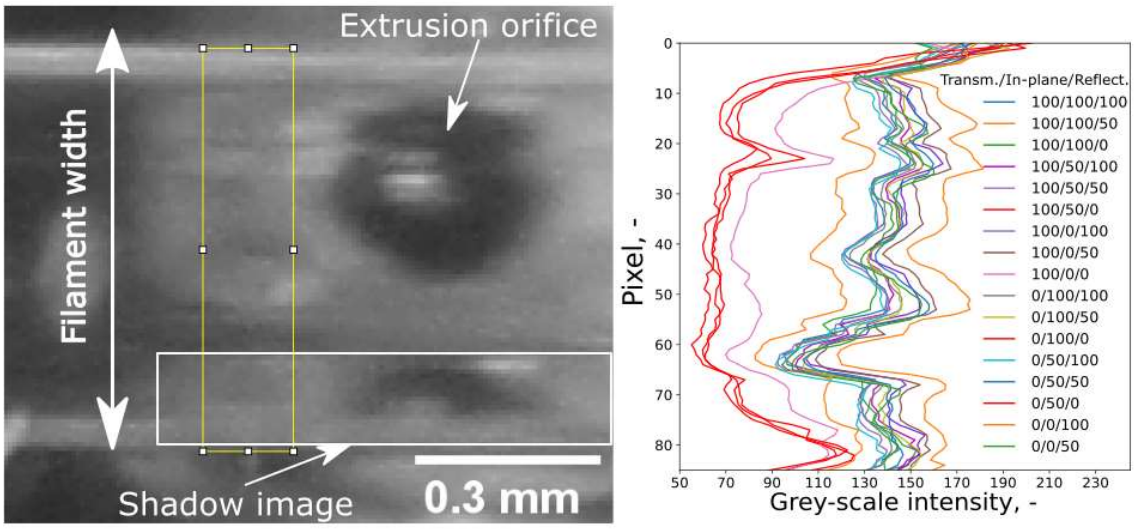

Figure 6: *In-situ* grey scale intensity (right) at different light conditions extracted at the middle ROI (left).

At first, one can notice that due to the limited depth of field and sample-mirror-camera miss alignments, the image is not in focus. Yet, interesting observations can be drawn. The lighting conditions that were magnifying the trough and peaks in the head ROI (absence of the nozzle), shown in red lines, are not suitable for the current case. This effect confirms the hypothesis that the nozzle reflects the light back to the sample as transmitted light. Also, one can observe that for the current case a phantom image is created below the extrusion orifice. This can be attributed to the out-of-focus image.

Finally, it is important to mention that the third region of interest, at the trailing of the filament, was also evaluated. However, once again, due to the camera-mirror-sample miss-alignment and limited depth of field, the images are blurry and unexploitable with current experimental procedure.

From these evaluations at the head ROI, the *in-situ* optical setup allowed to clearly image the interface between the filament and the bed substrate. Features of interest can be extracted in the images and the intensity profiles with optimized light conditions. The identification and characterization of these features are addressed in the next section. Nonetheless, important shortcomings are also identified linked to limits of the optical configuration for the focus and depth of field.

3.2 Ex-situ Observations

To characterize the nature of the features identified *in-situ*, conventional imaging was performed and used to compare the results obtained at the head and middle ROI. First, optical microscopy in a reflection mode was employed. Like for the *in-situ* observations, the optical microscope images were post-processed in imageJ. Figure 7 shows the measured grey-scale intensity across the filament at the head ROI. Due to the higher resolution of the optical microscope – in the order of 2.5 higher – when compared to the *in-situ* system, some finer features are here highlighted. Among this variety of fine features through the width of the filament (which are not visible in the *in-situ* observations), it interesting to notice the shark-skin effect.

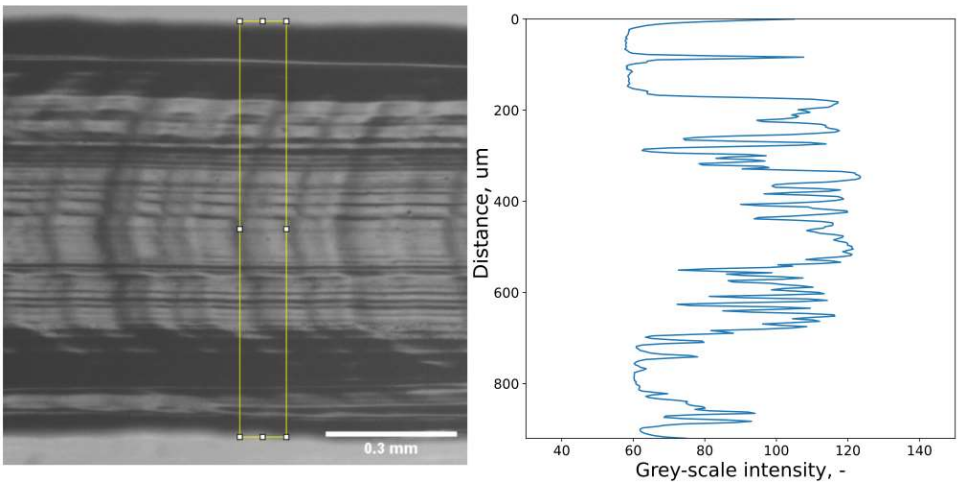

Figure 7: Grey-scale intensity (right) extracted from the optical microscope observation (left) at the head ROI. Like for the in-situ, the grey-scale intensity through the thickness is obtained by averaging the values inside the evaluation window. Dark/bright spots are identified by trough/peaks in the chart.

The shark-skin effect is referred to as a phenomenon in which the extruded polymer strands develop a regular surface pattern of ridges, resulting in an observable roughness. This effect is mainly attributed to a local stress concentration or stress singularity and polymer slippage at the nozzle exit, where there is an abrupt change in boundary conditions since the layer of the polymer melt close to the die surface accelerates abruptly from near-zero velocity to the average extrusion velocity of the filament. This leads to a stress and slippage singularity that is not withstood by the polymeric material, leading to surface cracking of the extrudate that repeats periodically, forming the shark-skin shape [9, 10], ultimately decreasing the contacting area between first-layer and bed.

By evaluating the shark-skin shape, it is believed that the dark regions (low grey-scale intensity) are related to a lack of contact between the first layer and the glass substrate. In order to confirm this hypothesis and determine the meaning of the observable features (dark vs bright regions), a confocal microscope was employed to generate a 3D map of the contacting interface. As shown in Figure 9, one can observe a large non-contacting band (colour map >> 0 µm) in the bottom of the image, which was also previously verified in a contrast of grey-scale signal in both, *in-situ* and optical microscope analysis. Also, it is possible to visualise the rough contact promoted by the shark-skin effect, reducing the contact signature between the first-layer and glass bed.

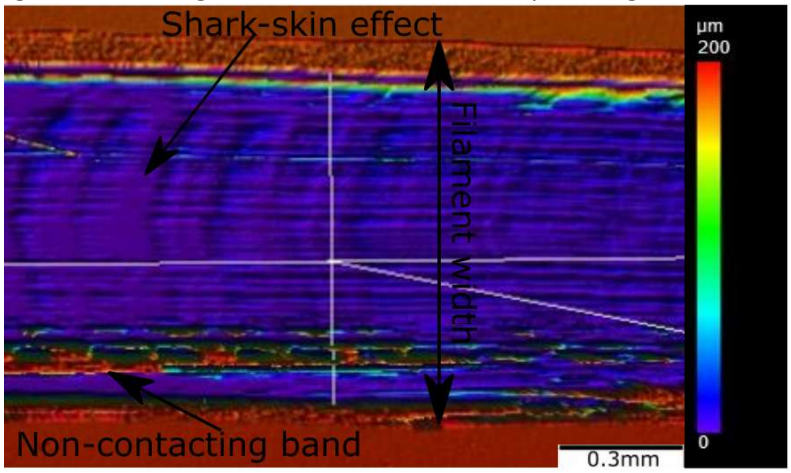

Figure 8: Confocal microscopy. 0µm zones are identified as areas that are into contact with the substrate. A large non-contacting band and shark-skin effect are observed. Those are key-features to be correlated with the in-situ and microscopy results.

The same procedure was repeated for the middle ROI. Figure 9 shows the microscope measured grey-scale intensity across the filament at the middle ROI. Once again, due to the higher resolution of the optical microscope when compared to the *in-situ* system, finer features through the width of the filament are observed. However, one can notice that the shark-skin effect observed at the head ROI is minimized, but still present, in the middle of the filament. This can be explained by the steady-state condition at this ROI, which is less impacted by kinematics-induced variations [11].

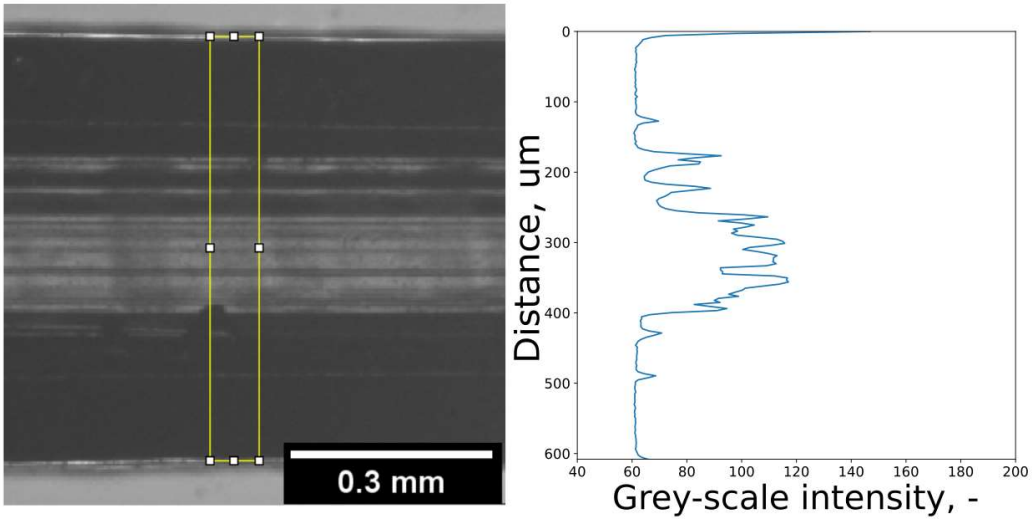

Figure 9: Grey-scale intensity (right) extracted from the optical microscope observation (left) at the middle ROI.

3.3 Method Comparison

The in-situ and ex-situ observations were compared. For the sake of a clear comparison, the [0/100/0] condition - which showed the highest peak-to-peak differences is used. The grey-scale signal extracted from the image obtained by the *in-situ* setup and the optical microscopy is shown in Figure 10. One can notice that similar global trends can be observed. However, the optical microscopy data shows more contrast and clear features, which is attributed to the shark-skin detection as a consequence of higher resolution of the later compared to the former.

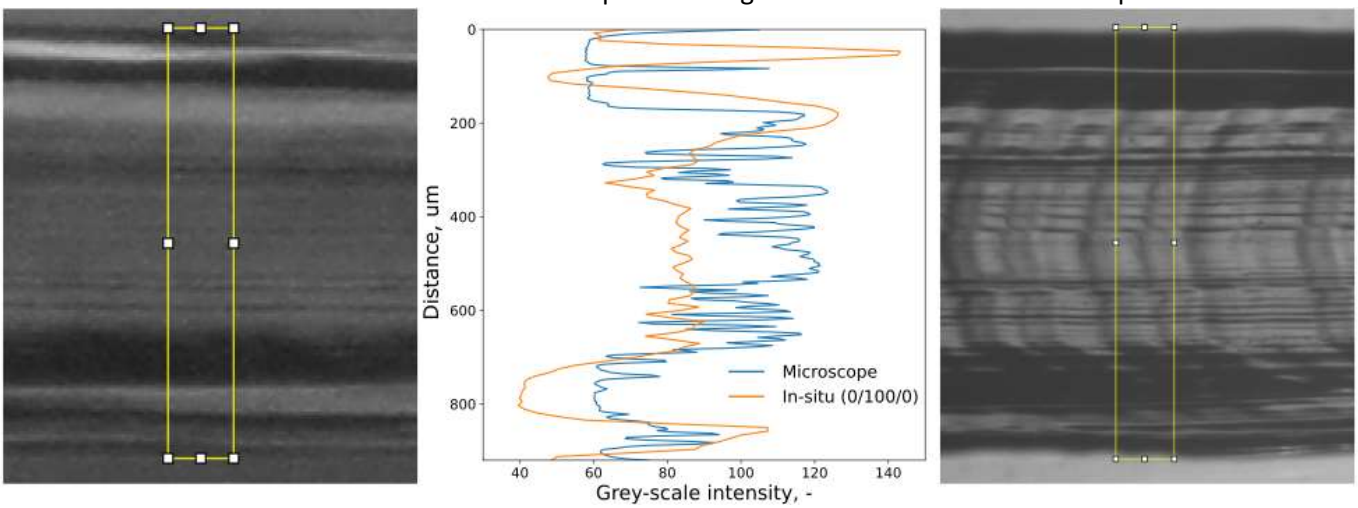

Figure 10: *In-situ* (left) vs optical microscope (right) imaging and their grey-scale response (middle) at the head of the filament. Signal comparison and correlation with dark/bright regions.

In order to translate grey-scale intensity into contact signature, the shark-skin effect found at the head ROI and shown in Figure 7 (optical microscope) and Figure 8 (confocal microscope) were compared. First, as expected, this comparison showed that the shark-skin effect leads to rough contacting zones. Secondly, it was possible to conclude that the regions with lower grey-scale intensity in the microscopy imaging (dark zones) corresponds to zones that are not in contact with the glass substrate. Therefore, since there is a good correlation between the *ex-situ* optical microscope measurements and the *in-situ* ones, it can be concluded that the zones with lower grey-scale intensity corresponds to zones that are not in contact with the glass substrate.

The *in-situ* and the *ex-situ* microscopy measurements at the middle ROI were compared. For this comparison, the [0/0/100] condition - which showed the highest peak-to-peak differences - is used. As shown in Figure 11, the grey-scale correlation is not as clear as the one found for the head ROI, given the fact of the out-of-focus image for the current case.

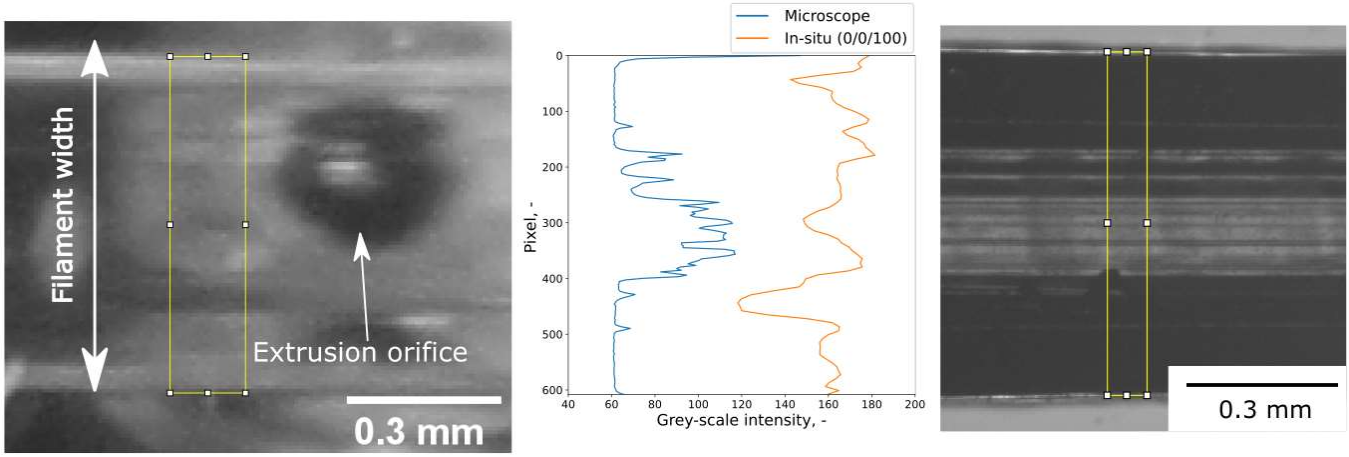

Figure 11: *In-situ* (left) vs optical microscope (right) imaging and their grey-scale response (middle) at the middle of the filament. Signal comparison and correlation with dark/bright regions.

4 CONCLUSIONS

Preliminary results of a novel *in-situ* optical technique to detect first-layer to substrate contact signature were presented, in which the signal intensities are highly dependent on the light conditions. *Ex-situ* methods, such as optical microscopy and confocal microscopy, were used to identify the features shown in the *in-situ* measurements.

Also, it was shown that the limited depth of field and camera-mirror-sample misalignment significantly impact on the quality of the *in-situ* data. Finally, it was shown that the light conditions that were suitable to evaluate the contact signature in the absence of the nozzle are not suitable when the nozzle is present. This is important to consider during a live, i.e dynamic, experiment.

Future work will focus on enhancing the setup, guaranteeing a proper alignment between the camera, mirror and sample. Also, obtaining better image resolution and increasing the depth of field will be addressed. Finally, the concept here described will be used to visualise, dynamically the evolution of the contacting signature in function of time.

5 ACKNOWLEDGEMENT

This work was funded by NSERC (Natural Sciences and Engineering Research Council of Canada) (grant number RGPIN-2018-03738). The authors would also like to acknowledge the assistance of Mr. Radu Romanica, Mr. Nabil Mazeghrane, Mr. Mohammad Saadati for their technical support.

REFERENCES

[1] H. Bikas, P. Stavropoulos, G. Chryssolouris (2015). "Additive manufacturing methods and modelling approaches: a critical review". The International Journal of Advanced Manufacturing Technology.

[2] D. Popescu, A. Zapciu, C. Amza, F. Baciu, R. Marinescu (2018). "FDM process parameters influence over the mechanical properties of polymer specimens: A review".

[3] H. Wu, Z. Yu, Y. Wang (2017). "Real-time FDM machine condition monitoring and diagnosis based on acoustic emission and hidden semi-Markov model". The International Journal of Advanced Manufacturing Technology.

[4] F.Li, Z. Z. Yu, Z. Yang, X. Shen (2020). "Real-time distortion monitoring during fused deposition modeling via acoustic emission".

[5] Z. Yang, L. Jin, Y, Yan; Y. Mei (2018). "Filament Breakage Monitoring in Fused Deposition Modeling Using Acoustic Emission Technique".

[6] C. Kousiatza, D. Karalekas (2016). "In-situ monitoring of strain and temperature distributions during fused deposition modeling process".

[7] Y. Li, W. Zhao, Q. Li, T. Wang, G. Wang (2019). "In-Situ Monitoring and Diagnosing for Fused Filament Fabrication Process Based on Vibration Sensors".

[8] K. Paraskevoudis, P. Karayannis and E. P. Koumoulos (2020). "Real-Time 3D Printing Remote Defect Detection (Stringing) with Computer Vision and Artificial Intelligence".

[9] J. Molenaar, R. J. Koopmans, and C. F. J. den Doelder (1997). "Onset of the sharkskin phenomenon in polymer extrusion".

[10] V Kishore1, C. Ajinjeru, P. Liu, J, Lindahl, A. Hassen, V. Kunc, C. Duty (2017). "Predicting sharkskin instability in extrusion additive manufacturing of reinforced thermoplastics". *28th Annual International Solid Freeform Fabrication Symposium.*

[11] J. Ren, A.T. Wei, Z. Jiang, H. Wang, and X. Wang (2021). "Improved Modeling of Kinematics-Induced Geometric Variations in Extrusion-Based Additive Manufacturing Through Between-Printer Transfer Learning"